Investigation of electromechanical properties in ferroelectric thin films using Monte Carlo simulation

Hai-Xia Cao[a)]
Department of Applied Physics, The Hong Kong Polytechnic University, Hong Kong, China and Department of Physics, Suzhou University, Suzhou 215006, China

Ven Cheong Lo
Department of Applied Physics, The Hong Kong Polytechnic University, Hong Kong, China

Winnie W. Y. Chung
Department of Applied Physics, The Hong Kong Polytechnic University, Hong Kong, China

(Received 11 August 2005; accepted 30 November 2005; published online 19 January 2006)

Electromechanical properties of ferroelectric thin films are investigated using a two-dimensional four-state Potts model and Monte Carlo simulation. In this model, the mechanical energy density induced by strains of individual cells is included in the system Hamiltonian, in addition to the contributions from dipole-dipole and electric-field-dipole couplings. Moreover, the dipole of each individual perovskite cell is aligned to one of the four mutually perpendicular directions. Four different states of dipole orientations can be defined. The deformation of each cell is associated with its dipole orientation, resulting in two different strain states. Polarization–electric-field hysteresis loops, butterfly loops for both transverse and longitudinal strains against electric field, as well as the phase-transition temperature under different stresses and anisotropy conditions are simulated. Results are comparable to the experimental measurements. © *2006 American Institute of Physics*. [DOI: 10.1063/1.2162269]

I. INTRODUCTION

Perovskite-type ferroelectric thin films have been extensively studied because of their applications in microelectromechanical systems (MEMS),[1–3] nonvolatile memory, microwave devices, and tunable dielectrics.[4,5] On one hand, the use of thin films promises superior device performance over bulk material. On the other hand, the physical properties of thin films are very different from the latter ones. As the film thickness is reduced, the interfacial effects from the film/electrode interface are increasing. One of these effects is the mechanical one induced by either thermal or lattice mismatch.[6–8] Due to the coupling between the electrical and mechanical energies, this interfacial effect, which may be otherwise ignored in a bulk sample, plays an important role on the electromechanical properties of thin films.

The traditional theoretical approach to study the electromechanical properties is by the Landau-Ginsburg free-energy expression, in power series of polarization and strain.[9,10] This approach has been successful in tackling the stress-induced phase transition and deriving electromechanical coupling coefficient. It is a macroscopic theory that might not be applicable to systems in nanometer scale. Experimental evidences suggest that the electromechanical properties are associated with the 90° domain-wall switching while 180°switching has little contribution.[11–13] A suitable theory to investigate the electromechanical properties must be the one capable of tackling 90° domain-wall switching. Four-state Potts model has been used previously to simulate ferroelectric properties.[14,15] In the present work, a two-dimensional four-state Potts model is used because it is capable to describe the microscopic switching mechanism.

For a single-crystalline (001)-oriented ferroelectric film in tetragonal phase, c domains are those regions with dipole orientation perpendicular to the film surface and a domains are those parallel to the surface. With the coexistence of both a and c domains, 90° domain walls exist even in single-crystalline samples. In addition, the influence of the substrate is important on the switching anisotropy, particularly, when the film thickness is small. For instance, it has been reported experimentally that the switching anisotropy is both thickness and temperature dependent.[16,17] The selection of bottom electrode material and its orientation are also important for the population of c domains.[18] The switching anisotropy itself on one hand reflects the preference of dipole orientation within the film, and on the other hand influences the strain distribution over a cell. In this work, the effect of switching anisotropy on the ferroelectric properties will be discussed. The next section is focused on the development of the model. The simulation results are presented in Sec. III.

II. MODELING AND SIMULATION

The system can be represented by a two-dimensional array of cells on the xz plane, with N_z cells along the z (or longitudinal) direction and N_x cells along the x (or transverse) direction. Because of the invariance of ferroelectric properties along the transverse (xy) plane, all kinetics along the y direction can be equally replaced by those along the x direction. Each tetragonal perovskite cell can also be replaced by a rectangle with two different edges c and a, where

[a)]Author to whom correspondence should be addressed; mailing address: Department of Applied Physics, The Hong Kong Polytechnic University, Hong Kong, China; electronic mail: hxcao@suda.edu.cn

 © 2006 American Institute of Physics

Downloaded 28 Mar 2011 to 158.132.161.9. Redistribution subject to AIP license or copyright; see http://jap.aip.org/about/rights_and_permissions

$c > a$. The dipole of each rectangle is along its elongated edge (or c edge). As has been presented previously,[14] a dipole at a location (i,j) can be represented by a pseudospin matrix $\hat{S}_{ij}$, which takes one of the four possible states (A, B, C, and D) to represent four different orientations,

$$\hat{S}_{ij} = \hat{S}_A = \begin{pmatrix} 1 \\ 0 \end{pmatrix} \quad (\text{along} + z \text{ direction}),$$

$$\hat{S}_{ij} = \hat{S}_B = \begin{pmatrix} 0 \\ 1 \end{pmatrix} \quad (\text{along} + x \text{ direction}),$$

$$\hat{S}_{ij} = \hat{S}_C = \begin{pmatrix} -1 \\ 0 \end{pmatrix} \quad (\text{along} - z \text{ direction}), \tag{1}$$

and

$$\hat{S}_{ij} = \hat{S}_D = \begin{pmatrix} 0 \\ -1 \end{pmatrix} \quad (\text{along} - x \text{ direction}),$$

where $0 < i \leqslant N_x$ and $0 < j \leqslant N_z$. The first element of each matrix represents the component along the z (longitudinal) direction, and the second along the x (transverse) direction. As the direction of the dipole is associated with the orientation of the rectangle, the strain state of a cell can be defined and associated with the spin states as follows:[19]

$$\hat{\varepsilon}_{ij} = \hat{\varepsilon}_a = \begin{pmatrix} \varepsilon_0 \\ -\varepsilon_0/2 \end{pmatrix}$$

$$(\text{for the pseudospin in either state } A \text{ or } C), \tag{2}$$

and

$$\hat{\varepsilon}_{ij} = \hat{\varepsilon}_b = \begin{pmatrix} -\varepsilon_0 \\ \varepsilon_0/2 \end{pmatrix}$$

$$(\text{for the pseudospin in either state } B \text{ or } D),$$

where ε_0 is the constant strain value. The magnitude of the transverse strain is half of that longitudinal value because of the invariance of volume upon deformation of the cell and the equivalence of deformation along the x and y directions. By incorporating the mechanical energy density, the system Hamiltonian can be written as

$$H = -\sum_{ij,km} J\hat{S}_{ij}^T\hat{S}_{km} - p_0\sum_{ij} \hat{E}^T\hat{S}_{ij} - \sum_{ij} \hat{\sigma}^T\hat{\varepsilon}_{ij} + H', \tag{3}$$

where $\hat{X}^T$ denotes the transpose matrix of $\hat{X}$, J the coupling coefficient between pseudospins, p_0 the dipole moment for each cell, and $\hat{E}$ and $\hat{\sigma}$ are the electric-field and stress matrices, respectively. Both of them can be either externally applied or internally generated. They are expressed as follows:

$$\hat{E} = \begin{pmatrix} E_z \\ E_x \end{pmatrix} \quad \text{and} \quad \hat{\sigma} = \begin{pmatrix} \sigma_\ell \\ \sigma_t \end{pmatrix}, \tag{4}$$

where E_z and σ_ℓ are the longitudinal components for electric field and stress, respectively. E_x and σ_t are their corresponding transverse values. Finally, H' is the additional contribution taking the effect of anisotropic switching into account, which will be elaborated later. In this work, it is assumed that the quantities J, $\hat{E}$, and $\hat{\sigma}$ are homogeneous over the film. The summation in Eq. (3) is over the nearest neighbors only, for simplicity.

TABLE I. The change in Hamiltonian $\Delta H'$ after switching between a domain and c domain.

	$\hat{S}_{ij}$ initially at state a or c	$\hat{S}_{ij}$ initially at state b or d
Before rotation	$-h_3(\phi_c - \phi_a)$	0
After rotation	0	$-h_3(\phi_c - \phi_a)$
$\Delta H'$	$h_3(\phi_c - \phi_a) > 0$	$-h_3(\phi_c - \phi_a) < 0$

The pseudospins of the system are initialized as described previously.[14] This ensures that the system is initially unpoled. Because of the association between spin states and strain states, the strain configuration of the system is also automatically initialized, resulting in nearly zero transverse and longitudinal strains. In order to simulate a finite thickness along the longitudinal direction, free boundary condition is applied for both the top ($j=1$) and bottom ($j=N_z$) surfaces. To simulate infinite size along the transverse direction, periodic boundary condition is adopted along the transverse direction.

The switching of dipoles and hence the distortion of cells are implemented by the 90° rotation of dipoles at domain walls because it is more energetically favorable.[20] Consequently, a dipole at a domain wall can be randomly selected. Whether it is allowed to rotate is governed by the Metropolis algorithm, as has been described elsewhere. The change in Hamiltonian ΔH upon rotation of the dipole can be divided into two parts,

$$\Delta H = \Delta H_0 + \Delta H'. \tag{5}$$

The first term on the right-hand side of Eq. (5) denotes the change in Hamiltonian without considering the anisotropic effect, while the second one reflects the anisotropic switching effect. The explicit form of H' in Eq. (3) can be written as

$$H' = -\sum_{ij} h_3(\phi_c - \phi_a)|\hat{n}^T\hat{S}_{ij}|, \tag{6}$$

where ϕ_c is the switching anisotropy parameter representing the probability for a dipole to be aligned along the z direction, $\phi_a = 1 - \phi_c$ the probability along the x direction, h_3 the energy barrier between a and c domains during switching, and $\hat{n}$ the unit matrix along the longitudinal direction. Supposed that a dipole $\hat{S}_{ij}$ is selected and rotates into another state denoted by $\hat{S}'_{ij}$, the change in Hamiltonian $\Delta H'$ becomes

$$\Delta H' = h_3(\phi_c - \phi_a)\{|\hat{n}^T\hat{S}_{ij}| - |\hat{n}^T\hat{S}'_{ij}|\}. \tag{7}$$

If c domains are dominant, i.e., $\phi_c > \phi_a$, the signs of $\Delta H'$ under different cases are shown in Table I. From this table, it reveals that it needs an amount of energy $h_3(\phi_c - \phi_a)$ in order to rotate a dipole from c to a domain. Conversely, an energy of $-h_3(\phi_c - \phi_a)$ is released by rotating the dipole from a to c domain. Consequently, the dipole aligned along the z axis is more energetically favorable in a c-domain-dominated

Downloaded 28 Mar 2011 to 158.132.161.9. Redistribution subject to AIP license or copyright; see http://jap.aip.org/about/rights_and_permissions

sample. For $\phi_c < \phi_a$, dipoles parallel to the film are more stable. The dominance of either c or a domain can be manipulated by the selection of substrate.

The longitudinal polarization can be obtained by the ensemble average of all the dipoles as follow:

$$P_3 = \frac{\sum_{ij} \{\hat{n}^T \hat{S}_{ij}\}}{N_x N_z}. \tag{8}$$

To calculate the dielectric susceptibility, a small amplitude longitudinal dc electric field is applied to the film. The overall polarization reaches a steady-state value. The variance of polarization is then calculated by the following expression:[21]

$$\chi_{33} = \frac{\partial P_3}{\partial E_3} = \frac{N_x N_z}{kT} \langle P_3^2 - \langle P_3 \rangle^2 \rangle. \tag{9}$$

where $\langle \cdots \rangle$ is the time average of a quantity after the steady-state condition has been attained. To simulate isothermal polarization—electric field and strain—electric-field butterfly loops, a longitudinal alternating electric field is applied to the system. The electric-field matrix can be expressed as follow:

$$\hat{E} = \begin{bmatrix} E_0 \sin(2\pi t/\Gamma) \\ 0 \end{bmatrix}, \tag{10}$$

Where E_0 and Γ are the amplitude and period of the electric field, respectively, and t is time. Both the period and time are scaled in terms of number of Monte Carlo steps (MCS) according to the following relations:

$$\Gamma_{\mathrm{MCS}} = \Gamma \frac{N_x N_z}{\Delta t}, \tag{11}$$

and

$$t_{\mathrm{MCS}} = t \frac{N_x N_z}{\Delta t}, \tag{12}$$

where Δt is the infinite small time step. The purpose of this scaling is to ensure that the computed results are not affected by selection of time step. Finally, the longitudinal and transverse strains can be calculated from the following expressions:

$$\varepsilon_\ell = \frac{1}{N_x N_z} \sum_{ij} \hat{n}^T (\hat{\varepsilon}_{ij} - \hat{\varepsilon}_{ij}^0), \tag{13}$$

and

$$\varepsilon_t = \frac{1}{N_x N_z} \sum_{ij} \hat{q}^T (\hat{\varepsilon}_{ij} - \hat{\varepsilon}_{ij}^0), \tag{14}$$

where $\hat{\varepsilon}_{ij}^0$ is the initial strain matrix for each cell, and

$$\hat{q} = \begin{pmatrix} 0 \\ 1 \end{pmatrix}$$

is the unit matrix along the transverse direction.

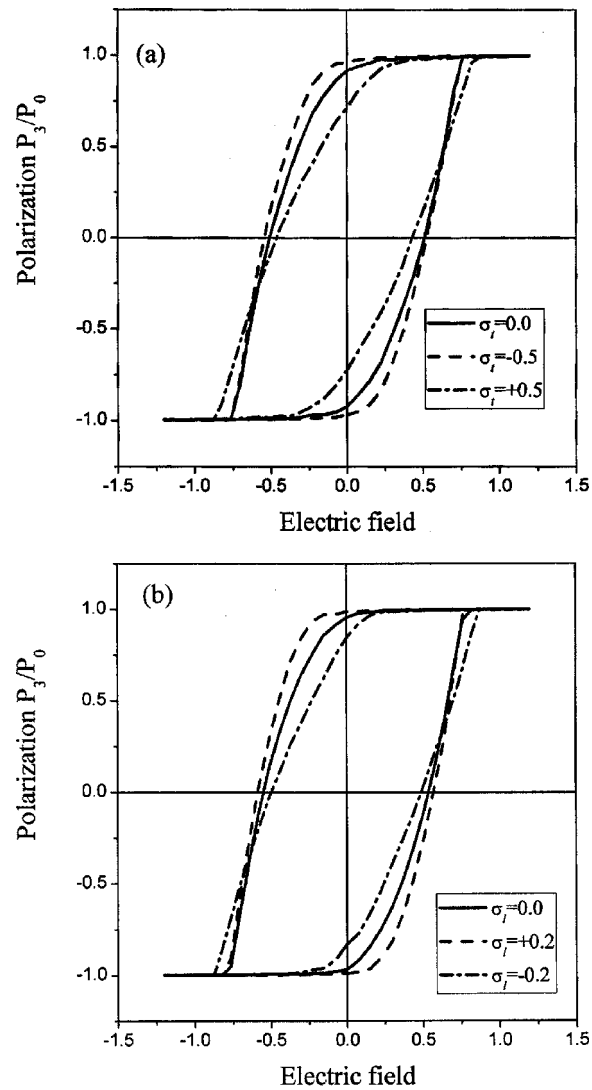

FIG. 1. Polarization vs electric-field hysteresis loops under different stress conditions (a) transverse stresses (σ_t=0.0, −0.5, and +0.5); and (b) longitudinal stresses (σ_ℓ=0.0, −0.2, and +0.2). Other parameters are Γ=400, E_0=1.2, T=1.0, ε_0=0.5, h_3=0.8, and ϕ_c=0.4.

III. RESULTS AND DISCUSSION

The polarization versus electric-field hysteresis loop, the butterfly loops for both longitudinal and transverse strains against electric field, and the susceptibility-temperature curve have been evaluated numerically under different static stresses and different switching anisotropy parameters ϕ_c. In our calculation, we have used the following parameters: Γ=400, E_0=1.2, T=1.0, ε_0=0.5, h_3=0.8, N_x=150, and N_z=80.

The polarization–electric-field hysteresis loops under different transverse and longitudinal stress conditions are shown in Figs. 1(a) and 1(b), respectively. The switching anisotropy parameter ϕ_c is 0.4. From Fig. 1(a), both the remanent polarization and coercive field are enhanced under the compressive stress ($\sigma_t < 0$) but are suppressed under tensile stress ($\sigma_t > 0$). On the other hand, from Fig. 1(b), both of these quantities are enhanced under a longitudinal tensile stress ($\sigma_\ell > 0$) but reduced under a compressive stress ($\sigma_\ell < 0$). The cause for the enhancement in longitudinal polar-

Downloaded 28 Mar 2011 to 158.132.161.9. Redistribution subject to AIP license or copyright; see http://jap.aip.org/about/rights_and_permissions

ization is that dipoles at both states A and C are encouraged while those at states B and D are hindered, which can be achieved either by applying transverse compressive stress or longitudinal tensile stress. The dominance of states B and D gives rise to the reduction of remanent polarization. The stability and enhancement of ferroelectricity by the dominance of c domains have been reported elsewhere in the literature.[22] For instance, Lynch[23] have investigated the electromechanical properties of ferroelectric films under different longitudinal compressive stresses. They concluded that the remanent polarization decreases with the magnitude of compressive stress. Zhou *et al.*[24] have obtained similar results. There has been so far no similar experimental report on the effect of transverse stress. We suggest that the longitudinal compressive stress and the transverse tensile stress are similar in suppressing dipoles in states A and C, which in turn reduces the remanent polarization. Furthermore, our result in Fig. 1(b) on the effect of longitudinal stresses can be directly compared with the above-mentioned experimental results. While it is difficult to introduce longitudinal tensile stress on the film, both the in-plane tensile and compressive stresses are possible. They can be easily manipulated by the selection of film/substrate combination, or bending the film in either concave or convex form.

The longitudinal and transverse strains, ε_l and ε_t, driven by an alternating longitudinal electric field are shown in Figs. 2(a) and 2(b), respectively, under different stress conditions and a fixed switching anisotropy parameter $\phi_c=0.4$. It is envisaged that the change in longitudinal strain over a cycle is larger (with smaller minimum value and the same saturated strain) under a transverse tensile stress. The corresponding change in transverse strain is also larger. Conversely, the transverse compressive stress yields the smallest changes for both strains. At $\phi_c=0.4$, the dipoles are preferentially aligned along the film (at both states B and D). The application of transverse tensile stress even enhances this preferential alignment. Under this situation, the transverse strain is the largest and the longitudinal one is the smallest. For each dipole at the domain wall, the switching from state B or D (a domain) to A or C (c domain) takes place only when a sufficiently large longitudinal electric field is applied. It follows by a decrease in transverse strain and an increase in longitudinal strain until the saturated strain values are attained. The switching then introduces large changes in strains for both directions. On the other hand, under a transverse compressive stress, nearly most of the dipoles are preferentially aligned along the z axis (at both states A and C) even in the absence of external electric field. The application of the longitudinal electric field does not affect so much on the alignment of dipoles. Consequently, the changes in strains are small. The presence of longitudinal stress produces exactly opposite trends on the changes in strains, as shown in Figs. 3(a) and 3(b), respectively. Zhou *et al.*[24] have investigated the electromechanical properties of the $Pb(Ni_{1/3}Sb_{2/3})O_3-PbTiO_3-PbZrO_3$ system by applying different longitudinal compressive stresses to the film. Both longitudinal and transverse strains against electric-field curves were obtained. Unlike our simulation, the saturated longitudinal strain decreases on increasing the compressive

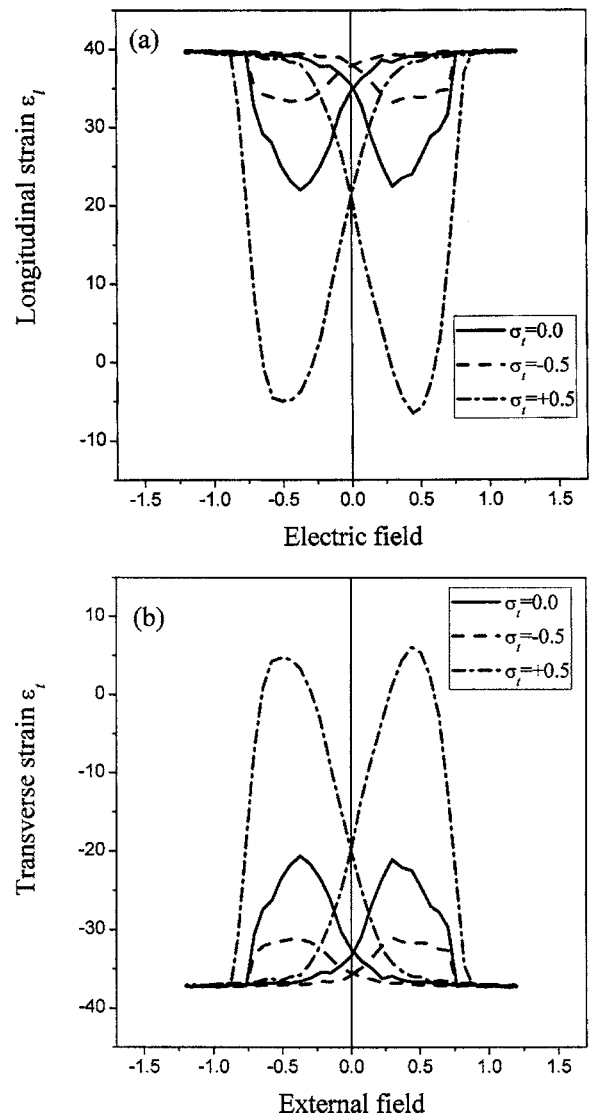

FIG. 2. (a) Longitudinal strain ε_ℓ and (b) transverse strain ε_t vs electric field under different transverse stresses (σ_t=0.0, −0.5, and +0.5). ϕ_c=0.4 for both graphs.

stress, while the saturated transverse strain increases. Moreover, the strain–electric-field butterfly loop is gradually enlarged on increasing the compressive stress and attains a maximum loop area when the stress value is about 25 MPa. The loop area then gradually shrinks and finally reduces to a horizontal line at a very large stress value. The shift in saturated strain is attributed to the elastic response, which has been omitted in our present calculation. The explanation of the variation of loop area with compressive stress is more complicated. It depends both on the initial domain configuration and ϕ_c. In general, the longitudinal compressive stress induces the dipoles to be preferentially aligned along the film (both states B and D), resulting in a small longitudinal strain and a large transverse strain. If the longitudinal external field is large enough, the dipoles can be switched to energetically favorable states, either state A or C, increasing the longitudinal strain but reducing the transverse strain. Consequently, an adequate longitudinal compressive stress can create larger changes in strains than under the unstrained case. On the other hand, if the compressive stress is too large, all dipoles

Downloaded 28 Mar 2011 to 158.132.161.9. Redistribution subject to AIP license or copyright; see http://jap.aip.org/about/rights_and_permissions

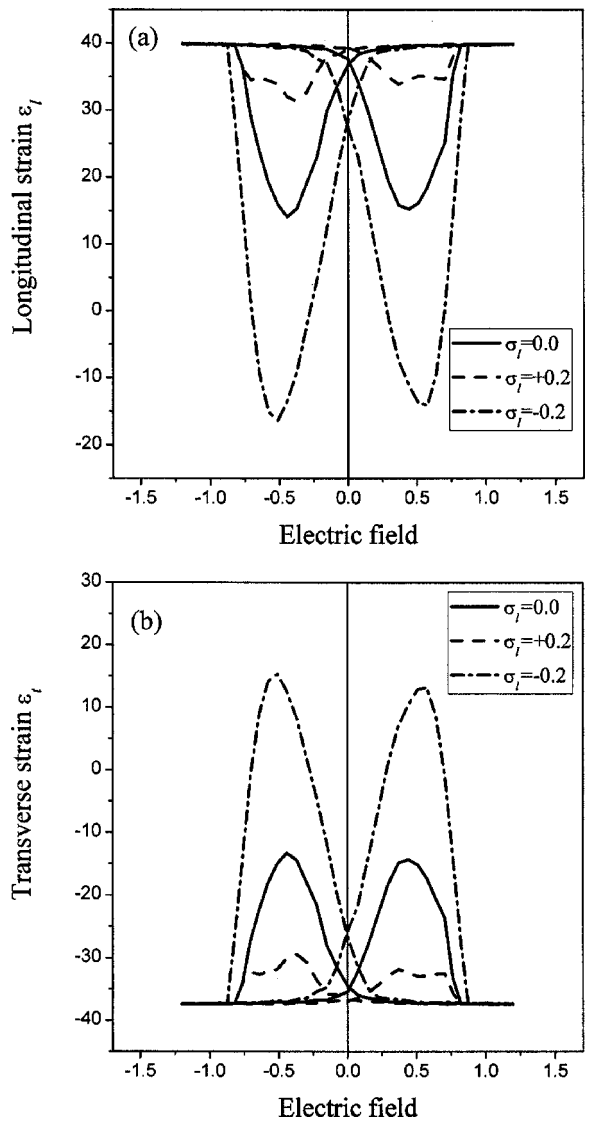

FIG. 3. (a) Longitudinal strain ε_ℓ and (b) transverse strain ε_t vs electric field under different longitudinal stresses (σ_ℓ=0.0, −0.2, and +0.2). ϕ_c=0.4 for both graphs.

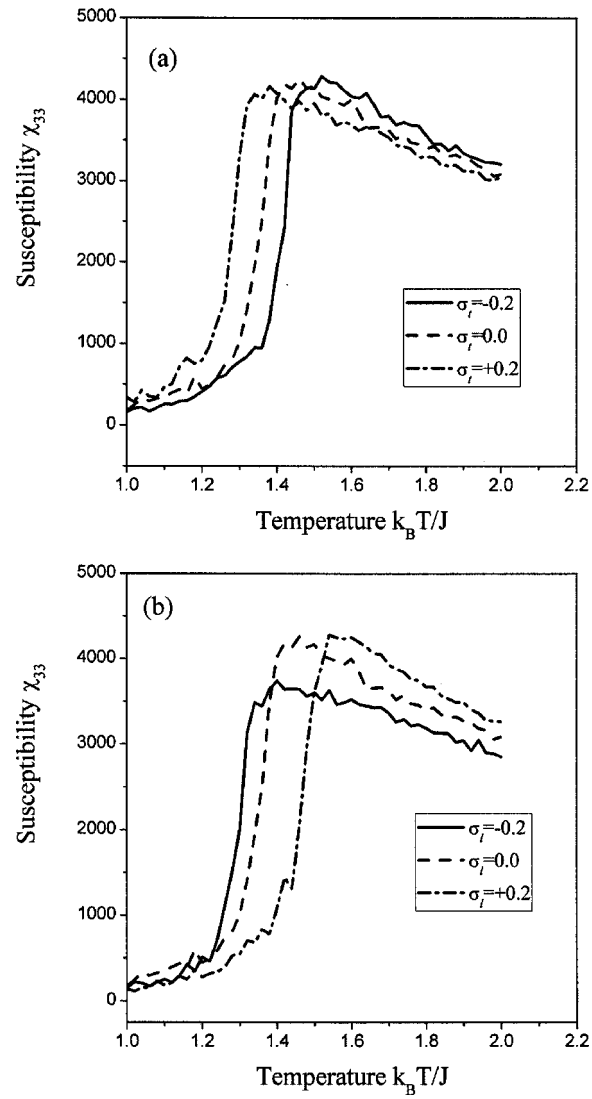

FIG. 4. Susceptibility vs temperature (a) under different transverse stresses (σ_t=0.0, −0.2, and +0.2), and (b) under different longitudinal stresses (σ_ℓ =0.0, −0.2, and +0.2). ϕ_c=0.55 for both graphs.

are clamped along the transverse direction that the switching is difficult. The butterfly curve then becomes smaller and finally constricts to a horizontal line.

The effects of transverse and longitudinal stresses on the phase-transition temperature are shown in Figs. 4(a) and 4(b), respectively. The phase-transition temperature can be determined by locating the peak position of the susceptibility-temperature curve. From these graphs, it can be concluded that the phase-transition temperature increases in a *c*-domain-dominated sample. This condition can be achieved by imposing either a transverse compressive or longitudinal tensile stress. Stress in opposite direction leads to the reduction of phase-transition temperature. Our result is qualitatively consistent with the other theoretical and experimental results. Lu and co-workers[25,26] have found that the Curie temperature was increased under a transverse compressive stress but was reduced under a tensile stress using Landau's free-energy approach. Rossetti *et al.*[27] have observed a 50 °C shift in the Curie temperature in a *c*-axis-oriented $PbTiO_3$ film under 400 MPa in-plane compression. Tenne *et al.*[28] investigated the influence of thermal strain on the vibration properties of polycrystalline $Ba_{0.5}Sr_{0.5}TiO_3$ using Raman spectroscopy. The thermal strain was induced by the thermal mismatch between the substrate and the film through the cooling from the deposition temperature to room temperature. Obviously, this strain must be parallel to the film surface. They concluded that the Curie temperature decreases when this strain is tensile. While our simulation result qualitatively agrees with all these experiments concerning the effect of transverse strain/stress on the shift in phase-transition temperature, our model can also be extended to the case of longitudinal stress.

The effects of switching anisotropy parameter ϕ_c on the longitudinal and transverse strains, and on the phase-transition temperature are shown in Figs. 5 and 6, respectively. In Fig. 5, the loop areas for the longitudinal and transverse strains are maximum when ϕ_c=0.4 and are minimum when ϕ_c=0.6. In other word, the loop area decreases with the switching anisotropy parameter ϕ_c. In Fig. 6, the phase transition temperature increases with ϕ_c. The effect of

Downloaded 28 Mar 2011 to 158.132.161.9. Redistribution subject to AIP license or copyright; see http://jap.aip.org/about/rights_and_permissions

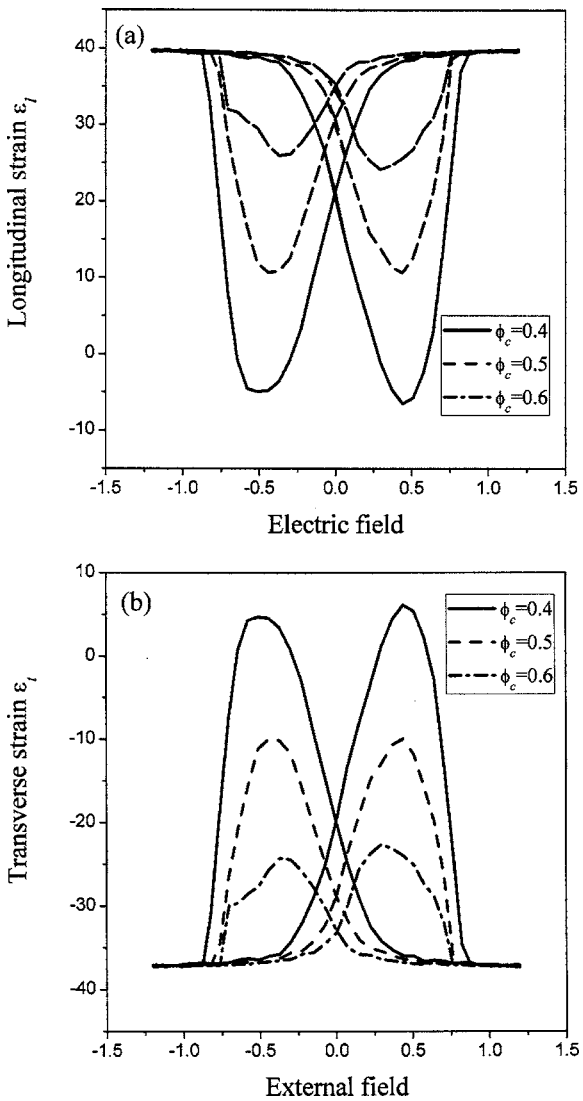

FIG. 5. (a) Longitudinal strain ε_ℓ and (b) transverse strain ε_t vs electric field under different ϕ_c values (σ_t=0.5).

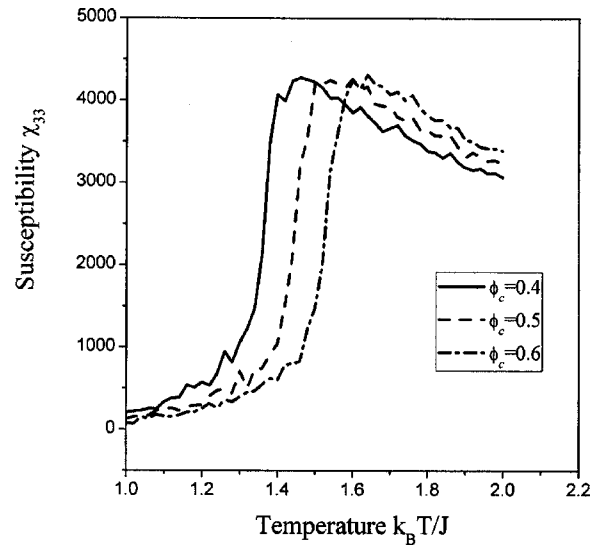

FIG. 6. Susceptibility vs temperature under different ϕ_c values (σ_t=−0.5).

switching anisotropy is to establish a preferential orientation along the longitudinal direction. Consequently, the volume fraction of *c* domains dominates under a high ϕ_c value. This dominance stabilizes the ferroelectricity, which can also be achieved by imposing either a longitudinal tensile stress or a transverse compressive one, as discussed before. Moreover, the combination of a transverse compressive stress and low ϕ_c value can yield the large loop area. The anisotropy parameter ϕ_c gives rise to unequal switching probabilities for a dipole from *c* to *a* and from *a* to *c* domains. The orientation dependence of various ferroelectric properties has been extensively studied in the literature, but its effect on phase-transition temperature has rarely been discussed. Among a few examples, Feng *et al.*[29] have shown the shift in phase-transition temperature from the permittivity versus temperature curves of ⟨001⟩-, ⟨011⟩-, and ⟨111⟩-oriented $0.62Pb(Mg_{1/3}Nb_{2/3})O_3$-$0.38PbTiO_3$ samples. However, the composition effect makes the interpretation difficult.

In our present calculation, we have simulated the effects of stress and switching anisotropy parameter on the electromechanical properties of ferroelectric films using a two-dimensional four-state Potts model, with the inclusion of a mechanical energy density in the system Hamiltonian. The coupling between the mechanical strain and dipole orientation is implemented by the association between the dipole state and strain state. However, there can be still a lot of improvement for this model. First of all, the presence of mechanical stress induces the deformation of a cell. This is an elastic response. This response causes the vertical drift in the strain–electric-field diagram, which will be further investigated in our next work. Secondly, there might be internal stress induced by the discontinuity of strain states across the film. This internal stress, in turn, might influence the dipole orientation in order to minimize the mechanical energy density. Consequently, an addition term to consider the coupling between the dipole of a particular cell and the strain states of its neighboring cells must be included.

IV. CONCLUSION

In summary, the electromechanical properties of the perovskite-type ferroelectric thin films have been numerically simulated using a two-dimensional four-state Potts model. Effects of stresses in different directions and switching anisotropy parameter ϕ_c on the polarization–electric-field hysteresis loops, butterfly loops for both transverse and longitudinal strains against electric field, as well as the phase-transition temperature, have been discussed. It was found that the ferroelectricity, in terms of remanent polarization and phase-transition temperature, can be enhanced by (i) the application of a transverse compressive stress, (ii) a longitudinal tensile stress, and (iii) high $\phi_c$value. Moreover, the maximum electromechanical response can be achieved by suitably applying the transverse tensile stress or the longitudinal compressive stress on the film.

ACKNOWLEDGMENTS

This work was supported by the Research Grant of the Hong Kong Polytechnic University under the Grant No. G-U032, the National Natural Science Foundation of China

Downloaded 28 Mar 2011 to 158.132.161.9. Redistribution subject to AIP license or copyright; see http://jap.aip.org/about/rights_and_permissions

under the Grant No. 10547129, and the Natural Science Foundation of JiangSu Education Committee of China under the Grant No. 04KJB140118.

[1]Q. F. Zhou, Q. Q. Zhang, T. Yoshimura, and S. Trolier-McKinstry, Appl. Phys. Lett. **82**, 4767 (2003).
[2]D. Kim, J. Maria, A. I. Kingon, and S. K. Streiffer, J. Appl. Phys. **93**, 5568 (2003).
[3]P. Gerber, C. Kügeler, U. Böttger, and R. Waser, J. Appl. Phys. **95**, 4976 (2004).
[4]H. N. Lee, D. Hesse, N. Zakharov, and U. Gosele, Science **296**, 2006 (2002).
[5]C. H. Ahn, K. M. Rabe, and J.-M. Triscone, Science **303**, 488 (2004).
[6]J. K. Lee, Y. H. Lee, K. S. Hong, and J. W. Jang, J. Appl. Phys. **95**, 219 (2004).
[7]R. Poyato, M. L. Calzada, and L. Pardo, Appl. Phys. Lett. **84**, 4161 (2004).
[8]T. R. Taylor, P. J. Hansen, B. Acikel, N. Pervez, R. A. York, S. K. Streiffer, and J. S. Speck, Appl. Phys. Lett. **80**, 1978 (2002).
[9]A. G. Zembilgotov, N. A. Pertsev, U. Böttger, and R. Waser, Appl. Phys. Lett. **86**, 052903 (2005).
[10]Z.-G. Ban and S. P. Alpay, J. Appl. Phys. **93**, 504 (2003).
[11]S. Li, W. Cao, A. S. Bhalla, U. Kumar, and L. E. Cross, *Proceedings of the 1990 IEEE Seventh International Symposium on Applications of Ferroelectrics* (IEEE, New York, 1991), p. 317.
[12]W. Zhang and K. Bhattacharya, Acta Mater. **53**, 185 (2005).
[13]E. Barcsu, G. Ravichandran, and K. Bhattacharya, J. Mech. Phys. Solids **52**, 823 (2004).
[14]K. T. Li and V. C. Lo, J. Appl. Phys. **97**, 034107 (2005).
[15]H. Qian and L. A. Bursill, Int. J. Mod. Phys. B **10**, 2027 (1996).
[16]N. A. Pertsev and A. G. Zembilgotov, J. Appl. Phys. **80**, 6401 (1996).
[17]V. Nagarajan, I. G. Jenkins, S. P. Alpay, H. Li, S. Aggarwal, L. Salamanca-Riba, A. L. Roytburd, and R. Ramesh, J. Appl. Phys. **86**, 595 (1999).
[18]K. S. Lee, J. H. Choi, J. Y. Lee, and S. Baik, J. Appl. Phys. **90**, 4095 (2001).
[19]W. F. Li and G. J. Wang, J. Appl. Phys. **91**, 3806 (2002).
[20]D. J. Kim, J. P. Maria, A. I. Kingon, and S. K. Streiffer, J. Appl. Phys. **93**, 5568 (2003).
[21]V. Privman, *Finite Size Scaling and Numerical Simulation of Statistical Systems* (World Scientific, Singapore, 1990).
[22]L. Lian and N. R. Sottos, J. Appl. Phys. **95**, 629 (2004).
[23]C. S. Lynch, Acta Mater. **44**, 4137 (1996).
[24]D. Zhou, M. Kamlah, and D. Munz, J. Eur. Ceram. Soc. **25**, 425 (2005).
[25]X. M. Lu, J. S. Zhu, Z. G. Liu, Z. S. Xu, and Y. N. Wang, Thin Solid Films **375**, 15 (2000).
[26]J. S. Zhu, X. M. Lu, P. Li, W. Jiang, and Y. N. Wang, Solid State Commun. **101**, 261 (1997).
[27]G. A. Rossetti, L. E. Cross, and K. Kushida, Appl. Phys. Lett. **59**, 2524 (1991).
[28]D. A. Tenne, A. Soukiassian, X. X. Xi, T. R. Taylor, P. J. Hansen, J. S. D. Speck, and R. A. York, Appl. Phys. Lett. **85**, 4124 (2004).
[29]Z. Feng, X. Zhao, and H. Luo, J. Phys.: Condens. Matter **16**, 6771 (2004).

Downloaded 28 Mar 2011 to 158.132.161.9. Redistribution subject to AIP license or copyright; see http://jap.aip.org/about/rights_and_permissions